Three-Dimensional Motion of the Organ of Corti

Werner Hemmert, Hans-Peter Zenner, and Anthony W. Gummer
University of Tübingen, Department of Otolaryngology, Section for Physiological Acoustics and Communication, 72076 Tübingen, Germany

ABSTRACT The vibration of the organ of Corti, a three-dimensional micromechanical structure that incorporates the sensory cells of the hearing organ, was measured in three mutually orthogonal directions. This was achieved by coupling the light of a laser Doppler vibrometer into the side arm of an epifluorescence microscope to measure velocity along the optical axis of the microscope, called the transversal direction. Displacements were measured in the plane orthogonal to the transverse direction with a differential photodiode mounted on the microscope in the focal plane. Vibration responses were measured in the fourth turn of a temporal-bone preparation of the guinea-pig cochlea. Responses were corrected for a "fast" wave component caused by the presence of the hole in the cochlear wall, made to view the structures. The frequency responses of the basilar membrane and the reticular lamina were similar, with little phase differences between the vibration components. Their motion was rectilinear and vertical to the surface of their membranes. The organ of Corti rotated about a point near the edge of the inner limbus. A second vibration mode was detected in the motion of the tectorial membrane. This vibration mode was directed parallel to the reticular lamina and became apparent for frequencies above ~0.5 oct below the characteristic frequency. This radial vibration mode presumably controls the shearing action of the hair bundles of the outer hair cells.

INTRODUCTION

The hearing organ achieves its extremely high sensitivity with an active, mechanical amplification process that is embedded in a three-dimensional (3D) structure—the organ of Corti. The central element is the outer hair cell (OHC), which can inject mechanical energy into the organ of Corti by axial contraction and elongation of its cell body (Brownell et al., 1985; Zenner et al., 1985). The OHC motion can follow a change of membrane potential, independent of frequency up to at least 20 kHz (Dallos and Evans, 1995; Frank et al., 1999). The transmembrane potential can be changed by a mechanical stimulus by shearing of the OHC stereocilia (Kros et al., 1992; Preyer et al., 1994, 1996) or perhaps by an electrical stimulus from extracellular microphonics (Dallos and Evans, 1995).

Here, we are interested in 3D mechanical properties of the organ of Corti, which influence the shearing motion of the OHC stereocilia. The shearing motion is governed by the relative motion between the reticular lamina (RL) and tectorial membrane (TM) (Fig. 1 *A*). The RL is coupled to the basilar membrane (BM) by the axial mechanical impedances of the OHCs (Neely and Stover, 1993) and the Deiters' cells (Nobili and Mammano, 1996), which support the OHCs on the BM (Fig. 1 *A*). Moreover, because the Deiters' cells are connected to the reticular lamina of more apically located neighboring OHCs by the phalangeal process, this longitudinal mechanical coupling might influence the motion of the stereocilia (Voldřich, 1983; Kolston and Ashmore, 1996). The tips of the longest stereocilia of the OHCs are embedded in the TM (Lim, 1980). The TM is coupled to the vibration of the RL by the OHC stereocilia and the narrow fluid layer of the subtectorial space. The geometry of the organ of Corti causes a transverse motion of the BM to be transformed into a radial (or shear) motion between the TM and the RL (Rhode and Geisler, 1967; ter Kuile, 1900). The TM possesses an additional vibration mode, predicted by Allen (1980) and Zwislocki and Kletsky (1979) and found experimentally by Gummer et al. (1996), which is a resonant vibration in the radial direction. According to Zwislocki (1980), this so-called parallel resonance is due to (a part of) the TM mass and the bending stiffness of the OHC stereocilia. This vibration mode will be influenced by the resistance of the narrow fluid layer of the subtectorial space (Allen, 1980; Zwislocki, 1980).

To investigate the micromechanics of the cochlear partition and to identify the different modes of vibration, a technique was developed to measure vibrations in mutually orthogonal directions. With present technology, such investigations are only possible in the apical part of the cochlea, where the surface of the organ of Corti is optically accessible. Due to the difficulties associated with maintaining this region of the cochlea in good physiologic and hydrodynamic condition (Cooper and Rhode, 1996), experiments were conducted in a temporal-bone preparation. The major problem with the temporal-bone preparation is that the endocochlear potential, which is an energy source for mechanoelectrical transduction, reduces to zero within 60

Received for publication 18 February 1998 and in final form 6 February 2000.

Address reprint requests to Anthony W. Gummer, University of Tübingen, Department of Otolaryngology, Section for Physiological Acoustics and Communication, Silcherstrasse 5, 72076 Tübingen, Germany. Tel: +49-7071-2984174; Fax: +49-7071-294174; E-mail: anthony.gummer@uni-tuebingen.de. Homepage: www.uni-tuebingen.de/cochlea.

Dr. Hemmert's present address is Massachusetts Institute of Technology, Building 36-865, 77 Massachusetts Ave., Cambridge, MA 02139. Tel: 617-258-5889; Fax: 617-258-5846; E-mail: whemmert@mit.edu.

© 2000 by the Biophysical Society

0006-3495/00/05/2285/13 $2.00

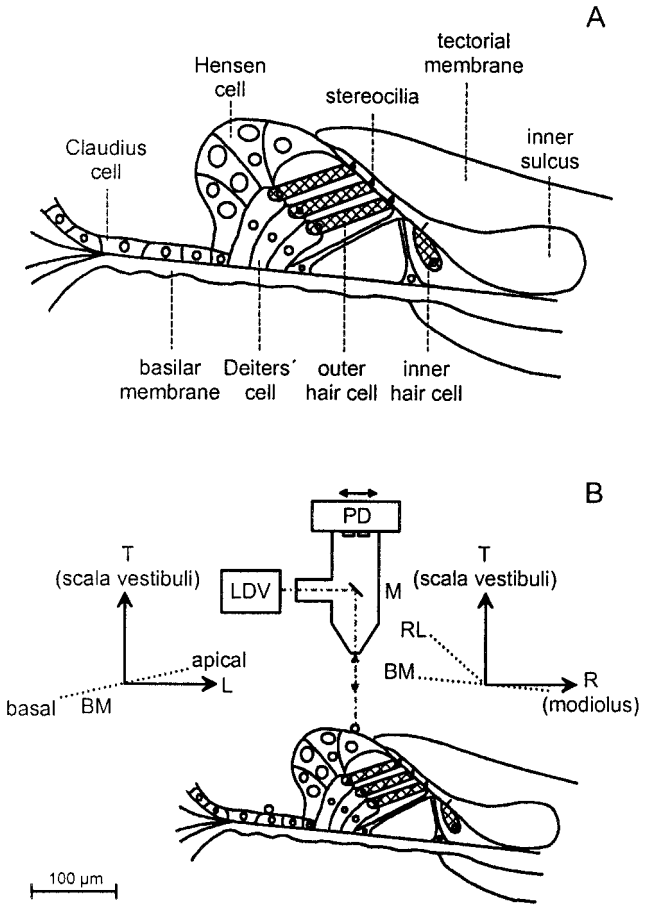

FIGURE 1 (*A*) Cross-section of the organ of Corti, showing outer hair cells, inner hair cell, Deiters' cells, Claudius cells, Hensen cells, basilar membrane, reticular lamina, tectorial membrane, stereocilia, and inner sulcus. (*B*) Coordinate system and the measurement set-up. The laser-Doppler vibrometer (*LDV*) measures velocity in the transverse direction, defined as being parallel to the optical axis of the microscope (*M*). The double photodiode (*PD*) measures displacement in the plane orthogonal to the transverse direction. The positions of the basilar membrane (*BM*) and the reticular lamina (*RL*) in the coordinate system (*R–L–T*) is marked with dotted lines. Note that the reticular lamina is inclined at about 35° to the basilar membrane. T, transverse; R, radial; and L, longitudinal directions.

min post mortem (Bosher, 1979). Only recently have in-vivo measurements of apical cochlear mechanics been published (Cooper and Rhode, 1993, 1995, 1996; Hao and Khanna, 1996; Rhode and Cooper, 1996; Ulfendahl et al., 1996; Maier et al., 1997; Zinn et al., 2000). The fact that, up to now, no significant differences in frequency selectivity between vibration responses measured in vivo and in vitro at the apical end of the guinea-pig cochlea have been found (Hemmert et al., 2000) justifies the use of a temporal-bone preparation to evaluate our new technique.

In this report, we describe properties of the 3D vibration of the organ of Corti, determined experimentally by optical measurements in three orthogonal directions. Preliminary reports of this work were presented at the Midwinter-Meeting of The Association for Research in Otolaryngology (Hemmert et al., 1995, 1997).

MATERIALS AND METHODS

Measurement set-up

A novel set-up was developed (Fig. 1 *B*) that allows the measurement of vibrations in three orthogonal directions by combining a laser-Doppler vibrometer (LDV, OFV-302: wavelength, 633 nm; output power, 1 mW; Polytec, Waldbronn, Germany) with a differential photodiode system with in-situ calibration. Both systems were coupled to an epifluorescence microscope (Aristomet, Leitz, Germany). The vibrometer measured velocity components in the transverse direction, whereas the photodiode was sensitive to displacements in the image plane, orthogonal to the laser beam. However, because bright-field illumination was required for the photodiode measurements, the two systems had to be used sequentially rather than simultaneously. To achieve high optical resolution and to avoid reflections from an air–water interface, a water-immersion objective lens with a high numerical aperture was used (Zeiss 40×: NA, 0.75; focal depth, 0.7 μm; working distance, 1.92 mm).

The LDV part of the set-up has been described elsewhere (Hemmert et al., 2000). Briefly, the fluorescence filter block of the microscope was replaced by a beam splitter (DLHS, modified, Spindler and Hoyer, Göttingen, Germany) to couple the laser light into the optical pathway of the microscope from the side. The beam splitter was designed to maximally reflect red light (550–730 nm; reflection coefficient at 633 nm, 99.8%), but allowed short-wave light (<550 nm) to transmit (60–98%). This concept allowed observation of both object and laser light when the preparation was illuminated from the side with a cold light source (KL 1500, Schott, Wiesbaden, Germany). The plane of the laser focus was adjusted to the focal plane of the microscope with the objective of the LDV. The LDV was mounted on a precision positioning stage (Spindler and Hoyer) to align the laser beam exactly with the optical axis of the microscope. The fine positioning of the laser focus on the desired cell was also performed with this system.

To yield a better image quality for the photodiode measurements, the beam splitter for the laser was withdrawn and additional bright-field illumination (100 W halogen lamp, DC-power supply) was used. The photodiode was mounted on a shielded piezoelectric bimorph that produced a reference signal of 246 nm when an electrical signal (1 V sine wave, 72.5 Hz) was applied. The sensitivity of the photodiode system was measured from this reference signal, allowing an in-situ calibration. Additionally, the reference signal gave an estimation for the linearity of the photodiode system, which was better than 1% for displacement amplitudes smaller than 250 nm. A double photodiode (BPX 48, Siemens, Fürth, Germany. photo-sensitive areas: width, $w = 0.7$ mm; length, $l = 2.2$ mm; distance between areas, $d = 90$ μm; spectral sensitivity: 430-1150 nm, with maximum at 850 nm) and differential amplifier (Gitter and Zenner 1995, modified) were used to obtain high sensitivity and rejection of illumination instabilities. The photodiode was inserted into the image plane of the microscope in a photo-adapter (magnification of objective and photo-adapter: 400×). Polystyrene microspheres (diameter, 10 μm; specific gravity, 1.05. Polyscience Inc., Warrington, U.S.A.) with high contrast were used to ensure sensitive recordings. The bimorph and photodiode were attached on a translation stage. The phototube of the microscope has two camera ports—the photodiode system was mounted in the focal plane on one of these ports. The translation stage allowed positioning of the photodiode over the image of the object.

Cochlear structures were documented with a CCD-camera (Hamamatsu C3077, Hamahita, Japan), with contrast enhancement (C2400). The camera was attached on the other camera port of the microscope's phototube. The image was displayed on a video monitor (total magnification: 3400×), onto which the position of the phododiode was marked. The second orthogonal direction in the horizontal plane was obtained by rotating the microscope's

phototube with photodiode and camera by 90°. Sections of the experiment were stored on a U-matic video system (Sony VO-7630). The temporal bone was fastened on a hydraulic micromanipulator (Narishige MO 103, Tokyo, Japan), which was mounted on a cardan joint to the microscope table. Like a set of goniometers, this system allowed the rotation of the object in three axes without loosing the focal point. The microscope table was equipped with micrometer screws to allow precise positioning. The whole microscope set-up was supported on a vibration isolation table (Vibraplane, Kinetic Systems, Roslindale, MA, U.S.A.) in a sound-attenuating chamber (IAC, Niederkrüchten, Germany).

When a water-immersion objective was used, the velocity signal measured with the LDV was corrected by a factor of 0.75 to account for the reduced speed of light in water. The frequency response of the low-pass filters (third-order Bessel filter, corner frequency: 5 kHz) in the Polytec controller (OFV 3000) and the time delay (19 μs) of the phase-locked loop (PLL)-velocity demodulator (OVD-01) were corrected. This was achieved by calibrating the laser system with a piezoelectric actuator (PSt 150/4/5, Pickelmann, München, Germany) with a high resonant frequency (50 kHz).

Velocity was defined positive for motion in the direction of scala vestibuli (T-component), the inner sulcus (R-component), and toward the apex (L-component). Sound pressure was positive for rarefaction. The velocity trajectories of the motion were extracted from the amplitudes and phases of the three orthogonal vibration components and plotted as elliptical projections. The displacement trajectories would show the same shape and direction, only their magnitudes would differ by a scaling factor of $1/2\pi f$.

The inclination of the organ of Corti relative to the measurement system was determined from the horizontal and transversal coordinates of landmarks: the surfaces of Claudius cells, Hensen cells and cells in the inner sulcus (Fig. 1). The distances between these points were measured on the monitor or with the micrometer screws of the object table. The plane of the BM was inclined to the focal plane of the microscope because of anatomical constraints of the preparation.

Frequency response measurement technique

To allow fast frequency-response measurements, band-limited pseudorandom noise was used, allowing determination of the complete frequency response curve within a single time window. This procedure relies on the system being linear, as it was found to be for levels less than 90 dB sound pressure level (distortion $<$ 1%). The stimuli were calculated for 2048 sample points, which were repeated every 20 ms and presented synchronous with the analysis window by the internal signal generator of the frequency analyzer (A&D 3525, Tokyo, Japan). For the measurements with the LDV, band-limited white noise (2.5–2 kHz, 800 spectral lines) was used. Because the dynamic range of the photodiode system was limited ($<$40 dB), a multitone signal was used, which had a reduced amplitude compared with white noise (10 dB). The frequency resolution of the signal was 6.3 spectral lines/oct; in later experiments, beginning with L154, 9.1 spectral lines/oct were used. The multitone signal was calculated by summing 44 (67) sinusoids with equal amplitude but random phase. All sinusoids were harmonics of 2.5 Hz, but with a minimum spacing of 6.3 (9.1) spectral lines/oct. Dividing the system's output by its input in the frequency domain, reveals both the amplitude and the phase of its transfer function at the frequencies where energy was provided. The multitone signal has the advantage that its maximum amplitude is a factor of 3 (3) and its total power is a factor of 18 (12) lower than that for band-limited white noise (800 spectral points). Moreover, for the same signal-to-noise ratio, the acquisition time is a factor of 44 (67) shorter than for sinusoidal stimulus paradigms.

Photodiode calibration

The transfer function and the frequency response of the photodiode system were determined with a microsphere glued on a piezoelectric actuator (PST 150/7/15, Pickelmann, resonant frequency: 25 kHz). The transfer function was measured with the actuator mounted in the horizontal plane and stimulated with a sinusoid (18 μm, 5 Hz). The output of the photodiode system as a function of displacement of the probe is shown in Fig. 2. For small amplitudes ($<$250 nm, shaded region in Fig. 2), the system was approximately linear (distortion $<$ 1%). To measure the frequency response, a multitone signal was used, and the photodiode signal was compared with the integrated velocity response of the piezoelectric actuator measured with the LDV. The frequency response of the photodiode exhibited a first-order low-pass function with a corner frequency of 550 Hz; this response was mathematically compensated.

Errors caused by nonlinearities of the photo-diode system when the broad-band multitone signal was used for frequency-response measurements were also mathematically estimated. For this purpose, the transfer function of the photodiode (Fig. 2) was approximated by a sinusoidal function. For 2% distortion (worst-case approximation), the calculated errors were less than 2 dB in amplitude and 5° in phase. Thus, provided that the photodiode was in its linear range (distortions in the reference signal smaller than 40 dB relative to the fundamental), errors in the frequency-response function caused by distortion could be neglected.

The accuracy of the photodiode measurements was limited predominantly by a slow drift of the preparation (velocity up to 30 μm/h on the tectorial membrane). To assess the change in photodiode sensitivity caused by this drift, the photodiode calibration was performed before and after the measurement of a displacement response. The amplitude was calculated using the geometric mean of the photodiode sensitivity, determined from the two reference measurements. The stability of the reference signal gave an estimation of the amplitude error of the photodiode measurement.

Preparation

Pigmented guinea pigs (250–400 g) with a positive Preyer's reflex were decapitated after cervical dislocation and the temporal bones removed rapidly. The bulla was opened widely to expose the cochlea ventrally, but leaving the middle ear intact. Ear drum and cochlea were moistened during the preparation with Hanks balanced salt solution (HBSS, Sigma, Deisenhofen, Germany; adjusted to 300 mOsmol and pH 7.4). The temporal bone was glued to a delrin cone where it was fastened on a ¼-inch microphone (B&K 4135). A piece of perforated parafilm was glued (Histoacryl) on the apex of the cochlea, onto which a droplet of HBSS was placed. Stria

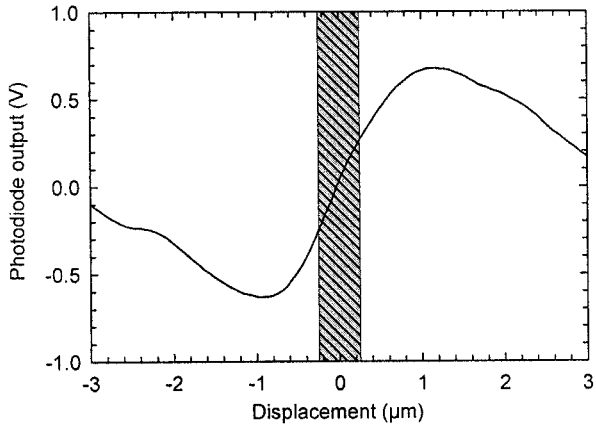

FIGURE 2 Output of the differential photodiode as a function of probe displacement. *Shaded area,* measurement region of ±250 nm.

vascularis was visible under the droplet with the preparation microscope (Wild M5A, 25 or 50× magnification). A hole (about 1 × 0.5 mm^2) was made in scala vestibuli without interrupting stria vascularis, the helicotrema or Reissner's membrane. For all measurements reported in this study, the cochlea was opened at a distance of ~2.3 mm from its apical extreme, corresponding to the 16-mm location (refer to von Békésy, 1960, Fig. 12-21).

To preserve the tectorial membrane, the droplet of HBSS was replaced by artificial endolymph (in mM: K^+ 150, Na^+ 1, Ca^{2+} 2, Cl^- 130, HCO_3^- 25, HEPES 5, pH 7.4, 300 mOsmol, according to Kronester-Frei, 1979) before Reissner's membrane was opened. In a series of experiments (L156–L164), a solution without Ca^{2+} (in mM: K^+ 150, Na^+ 1, Cl^- 126, HCO_3^- 25, HEPES 5, pH 7.4, 300 mOsmol) was used. However, the position of the tectorial membrane seemed not to be more stable in these preparations.

Polystyrene microspheres (diameter ~10 μm, specific gravity 1.05; Polyscience Inc., U.S.A.) were introduced into scala media to enable measurements on the low contrast surfaces of the BM and the tectorial membrane. Because polystyrene microspheres have almost the same specific gravity as water, they impose, in contrast to glass or metal particles, no additional mass loading to the cochlear structures. The water-immersion objective of the measuring-microscope was placed on the droplet. The cellular structures of the organ of Corti and the overlying beads were identified on the video display with contrast enhancement.

Sound system

Sound stimuli were delivered closed field from a DT 48 earphone (Beyer, Heilbronn, Germany) through a plastic tube damped with a woolen thread. The temporal bone preparation on the delrin cone was held by a ¼-inch condenser microphone (B&K 4135 and 2633 preamplifier, Naerum, Denmark) mounted on the cardanian joint on the microscope table. The microphone signal was amplified (B&K 2610, Denmark) and sent to the FFT-analyzer (A&D 3525, Japan). The signal produced by the generator of the FFT-analyzer was fed to an equalizer (Yamaha EQ-500, Tokyo, Japan) to correct, when necessary, for the frequency response of the loudspeaker. The frequency response of the sound stimulus was flat from 50 to 2000 Hz (±5 dB). All vibration responses were corrected for the sound pressure measured by the ¼-inch microphone near the ear drum and are given relative to 60 dB SPL.

Correction for the open cochlea condition

Alterations of the response characteristics of the cochlear partition due to the opening in the apex of the cochlea were corrected off-line by a similar procedure to the one proposed by Cooper and Rhode (1996). Because the correction procedure and its effects have been described in more detail elsewhere (Hemmert et al., 2000), the method is only briefly summarized here. The displacement response was inverse-Fourier transformed to yield the impulse response. Frequency components below 50 Hz, where the response was below the noise floor, were rejected. The impulse response consisted of a "fast" component, which was probably caused by the opening in the cochlea, and a "slow" component representing the traveling wave. The initial part of the impulse response, containing the fast component, was suppressed with a window with a $\cos^2$-shaped onset (rise-time, 1 ms); this, rather than a rectangular window, was used to reduce truncation artifacts. The total rise time was 1 ms. The time at half-maximum ($t_{1/2}$) of the window onset was about 1.8 ms in this cochlear region. For each preparation, $t_{1/2}$ was chosen by a process of trial-and-error. The delay $t_{1/2}$ was deemed as optimal when the notches in both the fast and slow responses disappeared. The end section of the impulse response (100–200 ms) was faded out by a window with a $\cos^2$-shaped decay (decay time, 100 ms). All recordings from one position were corrected with the same function. When the frequency response was measured with the multitone signal, the response spectrum was linearly interpolated to allow a reverse Fourier transformation. This procedure induced no significant loss in precision (compare Figs. 3 and 9): the differences of the corrected responses of the transverse component measured with white noise and the multitone signal was less than 2.4 dB, phase deviations were smaller than 8.6° (0.2–1 kHz).

Protocol for vibration measurements

The first vibration measurement was always carried out with the LDV. For measurements with the photodiode, bright-field illumination with the maximum available light intensity was used to obtain the highest signal-to-noise ratio. The reference signal for the bimorph was switched on, and the photodiode was positioned at the edge of the microsphere on the point of

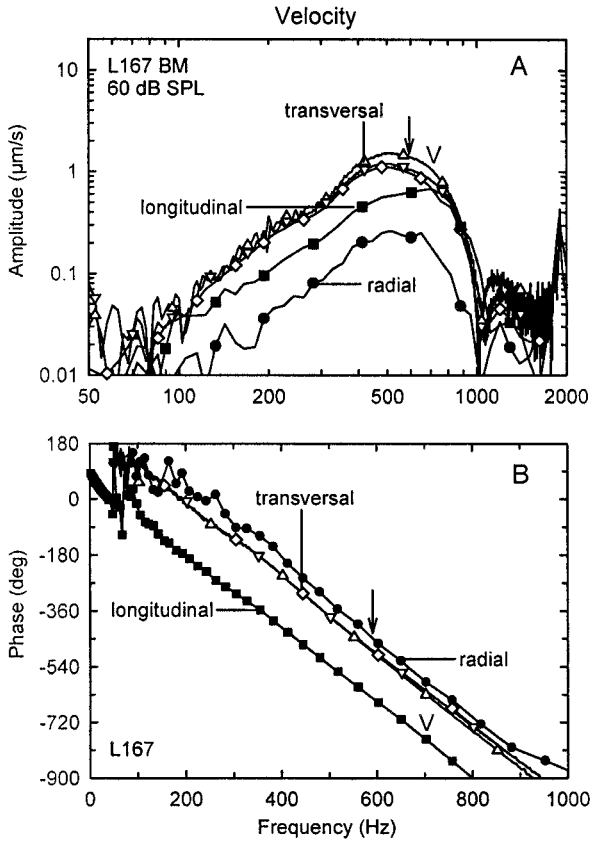

FIGURE 3 (*A*) Amplitude and (*B*) phase of the 3D velocity response of the BM, measured on a microsphere adhered to a Claudius cell on the surface of the BM. The transverse component (*open symbols*) was recorded before (*inverted triangles*) and after (*triangles*) the recordings in the focal plane and with the multitone signal (*diamonds*). Measurements in the focal plane were made with the differential photodiode (*filled symbols*) to obtain the radial (*circles*) and longitudinal (*squares*) components. Relative to the first measurement in the transverse direction (*inverted triangles*), measurements were made at 5 min (*longitudinal*), 7 min (*radial*), 12 min (*transverse, multitone signal*), and 14 min (*transverse, white noise*). The stability of the reference signal was ±5 dB for the radial component and ±0.3 dB for the longitudinal component. Notice that phases have been plotted on linear frequency axes so that pure delays are readily discerned as straight lines. The characteristic frequency of both the transverse and the radial components was 590 Hz (*arrow*); frequency of the maximum of the longitudinal component was 700 Hz (*arrowhead*).

maximum sensitivity. Care was taken that no other object of high contrast entered the receptive field of the photodiode. The reference signal was averaged (20×); the distortion components of the recordings were normally below the noise floor and at least 40 dB below the fundamental. For measurements with the photodiode, sound pressure levels of 90–100 dB SPL per frequency point were used to yield a sufficiently high signal-to-noise ratio. Care was taken that the vibration amplitude did not exceed that of the reference signal, so that the photodiode was still in its linear range. Again, 20 averages were recorded. To complete the measurements with the photodiode, a further reference measurement was recorded to estimate the stability of the object relative to the photodiode position. To measure the second orthogonal vibration component in the focus plane, the microscope's phototube with camera and photodiode was rotated by 90°, the object was realigned and the vibration recorded. Finally, another measurement with the LDV was made to document the stability of the object. In most experiments, the photodiode measurements were repeated once. No major differences were seen between the recordings.

RESULTS

Two-dimensional recordings (transverse and radial component) were performed in 11 preparations, and, in an additional 25 preparations, it was possible to conduct 3D vibration measurements. The fast component was successfully removed in 19 preparations, where 11 recordings were from the reticular lamina: 4 on the Claudius cells lying on the BM and 7 on the tectorial membrane. In this study, only the response characteristics of the slow component, attributable to the traveling wave response of the cochlear partition (Hemmert et al., 2000), are described.

Basilar membrane

An example of the three orthogonal velocity components of a microsphere on the Claudius cells covering the BM is plotted in Fig. 3. The transversal and the radial vibration components were tuned to ~590 Hz (*arrow*); the maximum of the longitudinal component was ~700 Hz (*arrowhead*). The frequency of 590 Hz represents the frequency at which the amplitude begins to rapidly decay; in keeping with convention (Wilson and Johnstone, 1975; Gummer et al., 1987; Hemmert et al., 2000), this frequency will be referred to as the characteristic frequency (CF). Unless specified to the contrary, the term CF will be reserved for the transverse component.

To document the stability of the preparation, the transversal vibration was measured before and after measuring the components in the orthogonal plane. The amplitudes in the CF region fell by no more than 3.7 dB (400–900 Hz); phase reductions were less than 10° (200–800 Hz). Measurements of the transverse component with band-limited white noise and with the multitone signal are also shown. The interpolated response to stimulation with a multitone signal showed no significant differences to those of the responses measured with white noise. The amplitude deviations were smaller than 2.4 dB and the phase differences were smaller than 7.3° (200 Hz–1 kHz).

The calibrating reference signal, generated by vibrating the photodiode, fell by ~10 dB during the measurement of the radial component because of a 500-nm drift in the position of the microsphere relative to the photodiode—this drift is small compared with the diameter of the microsphere (10 μm). The amplitude of the radial component was 15 ± 5 dB below the transverse component. The phase of the radial component led that of the transverse component by 42° (400–800 Hz). The reference signal was stable (±0.3 dB) during the measurement of the longitudinal component. The amplitude of the longitudinal component was about 6 dB below the transverse component ($f <$ CF) and almost in antiphase to it, lagging by 160° (400–800 Hz).

The amplitude and phase data of the three orthogonal vibration components can be used to reconstruct the trajectory of the motion. The motion of each point can be plotted as an elliptical projection. Fig. 4 shows the projections of the velocity trajectories in the R–T and L–T planes. The trajectories in the R-T-plane were almost rectilinear, with the major axis at an angle of 80° to the R-axis (Fig. 4 *A*), independent of stimulus frequency. Considering the measurement uncertainty of the radial component of ±5 dB, the true angle is expected to be somewhere between 72° and

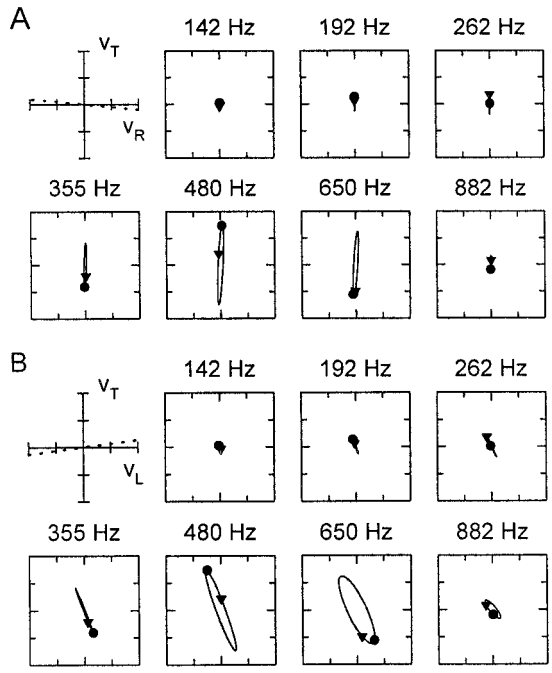

FIGURE 4 Velocity trajectories of a microsphere on the BM in the (*A*) R–T-plane and (*B*) L–T-plane at different frequencies. Data are from Fig. 3. Inclination of the BM was 354° to the R-axis and 8° to the L-axis (*dotted lines*). The tags on the ellipses at $t = 0$ (*circles*) and $t = T/4$ (*triangles*) allow determination of the direction of motion. For the R–T-plane, the instability of the reference signal (±5 dB) caused an uncertainty of the angle of the trajectories of about ±6°. For the L–T-plane, the accuracy of the angle of the trajectories was limited mainly due to the decrease of the transverse component (<3.7 dB), giving an uncertainty of less than ±10°. The scale bars extend to ±2 μm/s.

84°. In this preparation, the BM was inclined at −6° to the R-axis, so that its motion was approximately orthogonal to this axis. In the L–T plane, the elliptical trajectories were more opened (Fig. 4 *B*)—the direction of the major axis of the motion was 116°, also independent of frequency. The BM was inclined at 8° to the L-axis, so that the motion was approximately orthogonal to this axis. Taken together, the two sets of data imply that the direction of motion was orthogonal to the surface of the BM at all frequencies. Averaged over all preparations, no significant difference in CF between transverse and longitudinal (0.11 ± 0.16 oct, $N = 4$) or between transverse and radial (−0.07 ± 0.10 oct, $N = 5$) components were found on the BM.

Hensen cells

In some preparations, it was also possible to conduct 3D measurements of the motion of a microsphere located on a Hensen cell (Fig. 5) after the BM recordings (Fig. 3). The bead was located close to the OHC, as depicted in Fig. 1 *B*. For the preparation illustrated here, both sets of data were recorded over a period of 30 min. The CF was 490 Hz, rather than 590 Hz as found on the BM. The amplitude of the radial vibration component was ~2 dB larger than the transverse component; the phase-difference was 13° (200–800 Hz). The longitudinal component was more sharply tuned ($Q_{10dB} = 1.2$) than the transverse and radial components ($Q_{10dB} = 0.8$ and 0.9, respectively); it was tuned to 700 Hz, like the BM in the longitudinal direction. Its amplitude was 10–20 dB lower than the transverse component ($f <$ CF), but, above CF, it was higher (2 dB). The longitudinal component lagged the transverse component by 142° (200–800 Hz).

The velocity trajectories for the Hensen cell are shown in Fig. 6. The RL was inclined 140° to the R-axis (Fig. 6 *A*); this was determined by measuring the relative position of the focus on the inner sulcus and the surface of the Hensen cell. The BM was inclined at 354° to the R-axis. The major axis of the trajectories in the R–T plane was about 38° for all frequencies (Fig. 6 *A*). This means that, within the limits of measurement accuracy, the direction of motion of the Hensen cell was orthogonal to the surface of the RL at all frequencies (largest deviation, 12°). The ellipses opened wider with increasing frequency up to the CF because of the accumulating phase-difference between the two components. In the L–T plane (Fig. 6 *B*), the angle of the major axis was between 95° and 102° at CF. The direction of the vibration was therefore approximately orthogonal to the reticular lamina for frequencies up to CF. In contrast to the situation in the R–T plane and to the case of the BM, the major axis rotated (counterclockwise) away from the orthogonal at frequencies above CF, amounting to about 30° at the frequency of the maximum of the longitudinal component.

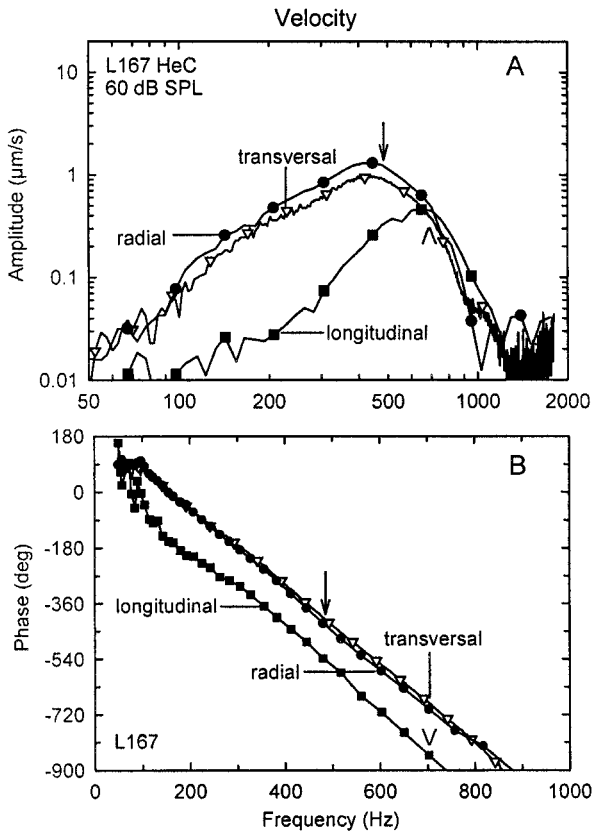

FIGURE 5 (*A*) Amplitude and (*B*) phase of the 3D velocity response of a microsphere on a Hensen cell (close to the outer hair cell). The transverse component (*triangles*) was recorded after recording the radial (*circles*) and longitudinal (*squares*) components. These responses were recorded after the responses on the BM, which were shown in Fig. 3. Relative to the measurement in the radial direction, measurements were made at 3 min (*longitudinal*) and 7 min (*transverse*). The measurement in the radial direction on the Hensen cell was made 40 min after the first measurement in the transverse direction on the BM. The stability of the reference signal was ±0.2 dB for the radial component and ±0.4 dB for the longitudinal component. CF of both the transversal and radial components was 490 Hz (*arrow*); the frequency of the maximum of the longitudinal component was 700 Hz (*arrowhead*).

The estimates of the directions of motion of the BM and RL are consistent with the geometry of the organ of Corti. The difference between the major axes of their motion ranged from 35° to 45°, which is approximately equal to the physical angle between the two membranes. Moreover, their motion was parallel in the longitudinal direction (up to CF).

To illustrate differences between recordings from different animals, the velocity responses and associated trajectories for another Hensen cell are shown in Figs. 7 and 8, respectively. In contrast to the situation for the Hensen cell illustrated in Figs. 5 and 6, the response curves for all three orthogonal components were of the same shape with similar Q_{10dB} and CF. The phase differences between the transverse and the radial components was 19°, between the transverse and the longitudinal components 205°. Moreover, the tra-

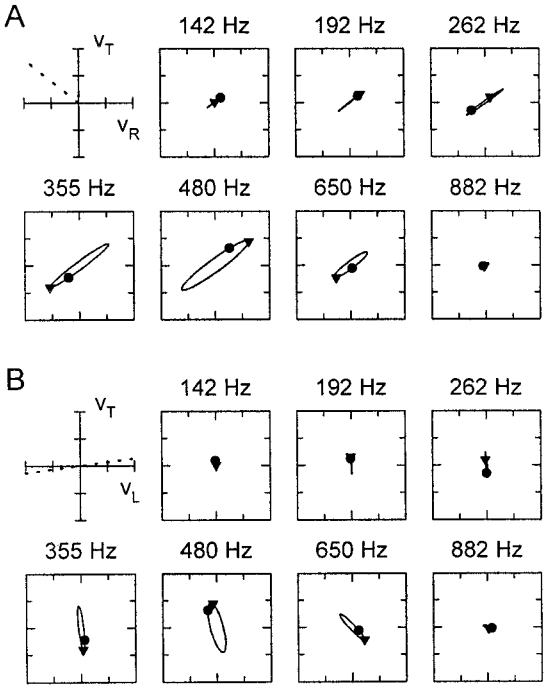

FIGURE 6 Velocity trajectories of a microsphere on a Hensen cell in the (*A*) R–T-plane and (*B*) L–T-plane at different frequencies. Data are from Fig. 5. Inclination of the RL was 140° to the R-axis and 8° to the L-axis (*dotted lines*). The scale bars extend to ±2 μm/s.

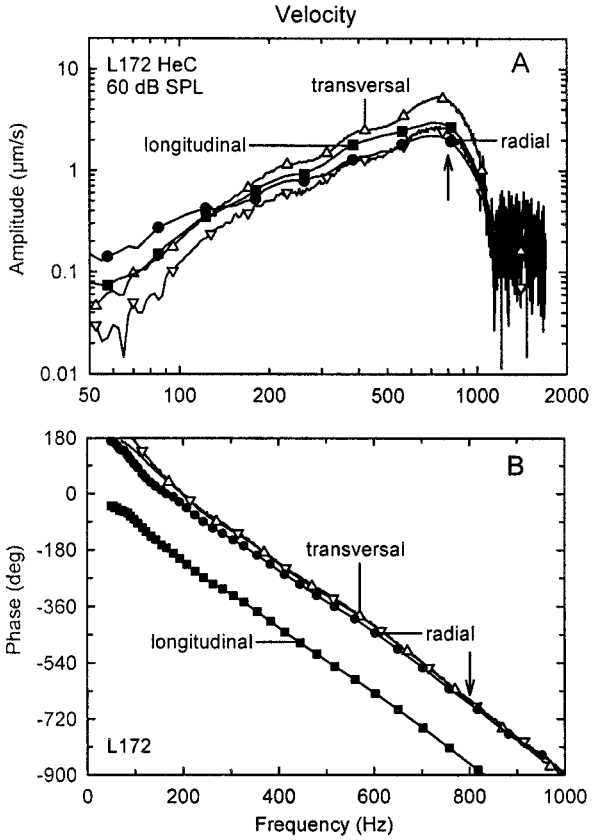

FIGURE 7 (*A*) Amplitude and (*B*) phase of the 3D velocity response of a microsphere on a Hensen cell. The transverse component was recorded before (*triangle*) and after (*inverted triangles*) recording the radial (*circles*) component; the longitudinal component (*squares*) was recorded thereafter. Relative to the first measurement in the transversal direction, measurements were made at 7 min (*radial*), 13 min (*transverse*), and 16 min (*longitudinal*). The stability of the reference signal was ±2 dB for the radial component and ±1.2 dB for the longitudinal component. The CF was 800 Hz for all components (*arrow*).

jectories of motion were almost rectilinear and orthogonal to the RL at all frequencies.

Tectorial membrane

The vibration of the TM in the transverse and radial directions is illustrated in Fig. 9. The transverse component was measured before and after the radial component. The reference signal generated by the vibration of the photodiode was stable (±0.5 dB). For the later measurement in the transverse direction, the amplitudes had fallen by 7.6 dB over the whole frequency range; however, the phase reductions were only 11° (200–800 Hz), much smaller than the phase difference between the transverse and radial components, which was as high as 60°.

The transverse vibration component was tuned to about 650 Hz; the maximum of the radial component was at 550 Hz. The phase of the radial component relative to that of the transverse component was small for frequencies well below CF (20° at 200 Hz). Beginning at ~0.5 oct below CF, the relative phase steadily increased, reaching 60° at 608 Hz, close to CF. Therefore, the trajectories of the motion (Fig. 10) were almost rectilinear for frequencies well below CF and became almost circular just below CF. The angle of the major axis to the R axis was between 60° and 70° (200–700 Hz). (The orientation of the BM was approximately horizontal in this preparation). In conclusion, these trajectories indicate a second vibration mode, evident for frequencies above ~0.5 oct below CF and directed approximately parallel to the reticular lamina.

DISCUSSION

Three-dimensional vibration measurements were conducted by combining an in-situ calibrated photodiode system and an LDV. The vibrometer detected motion in the transverse direction, whereas the photodiode system detected motion in the plane orthogonal to the transverse direction. The sensitivity of the photodiode (noise floor: 2–5 nm/$\sqrt{\text{Hz}}$ at 100 Hz; 0.67–1.7 nm/$\sqrt{\text{Hz}}$ at 1 kHz) was less than for the LDV (noise floor: 0.15–0.75 nm/$\sqrt{\text{Hz}}$ at 100 Hz; 0.015–0.075 nm/$\sqrt{\text{Hz}}$ at 1 kHz). Additionally, the dynamic range of the photodiode was limited to 40 dB for displacements up to 250 nm (magnification: 400×), whereas it was greater than 66 dB up to 2 μm for the vibrometer. However, it is

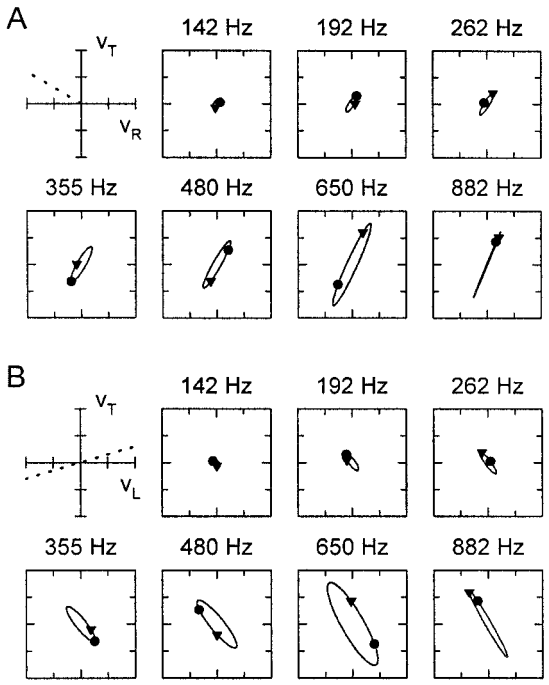

FIGURE 8 Velocity trajectories of a microsphere on a Hensen cell in the (*A*) R–T-plane and (*B*) L–T-plane at different frequencies. Data are from Fig. 7. Inclination of the RL to the R-axis and L-axis were, respectively, 4° and 17° (*dotted lines*) and, for the BM, the inclinations were 145° and 17° (*doted lines*). The scale bars extend to ± 2 μm/s.

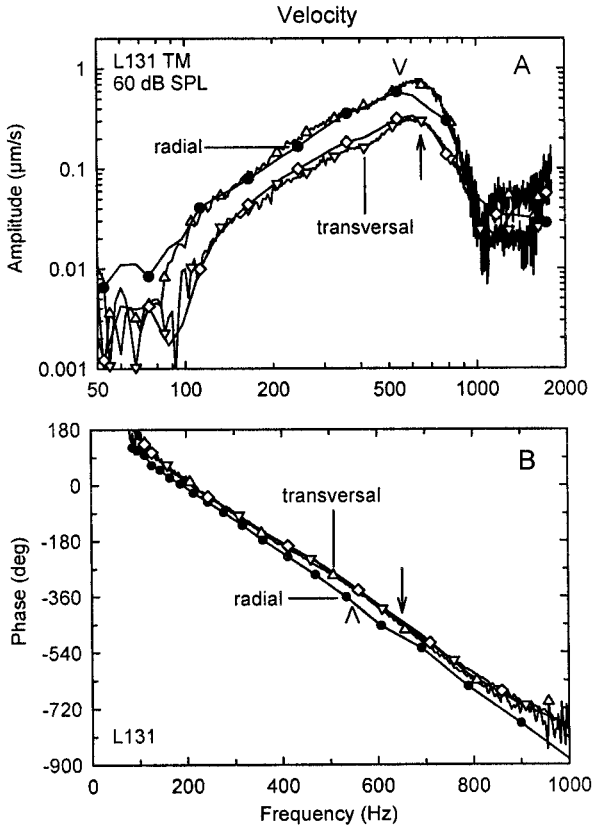

FIGURE 9 (A) Amplitude and (*B*) phase of the two-dimensional velocity response of a microsphere on the tectorial membrane. The transverse component was recorded before (*triangles*) and after (multitone signal, *diamonds*; white-noise, *inverted triangles*) recording the radial (*circles*) component. Relative to the first measurement in the transversal direction, measurements were made at 13 min (*radial*), 15 min (*transverse*, multitone signal) and 16 min (*transverse*, white noise). The stability of the reference signal was ± 0.5 dB for the radial component. The CF was 650 Hz for the transverse component (*arrow*); the frequency of the maximum of the radial component was 550 Hz (*arrowhead*).

possible to increase the linear range of the photodiode by reducing the magnification. The contrast was larger for microspheres on Hensen cells than on the BM because stria vascularis and the overhanging organ of Corti reduced the effective aperture of the objective. The photodiode was rotated by 90° to make the two sets of orthogonal measurements in the focal plane. An obvious improvement in this respect could be achieved by replacing the differential photodiode with a four-quadrant diode array. This would allow the simultaneous recording of the two orthogonal components in the focus plane (provided that a measurement system with sufficient input channels is also available). To obtain maximum sensitivity for recordings with the photodiode, reflecting microspheres were placed on the objects to be measured, making the procedure invasive. Nevertheless, the advantage of this system is that it allows vibration measurements along three mutually orthogonal axes without the need for rotating the object under consideration.

An alternative method was published by Decraemer et al. (1994) and Ulfendahl et al. (1995). They measured the vibration with a single-point laser Doppler interferometer and rotated the object to the desired recording direction. From recordings from at least three linear-independent directions, it is possible to calculate the three orthogonal vibration components and thereby reconstruct the 3D motion of the object. A disadvantage of such a method for their applications is the limited viewing angle caused by anatomical constraints, meaning that the object can only be rotated by small amounts. Decraemer et al. (1994) were able to access the umbo from an angle of only ± 15. The viewing angle is also restricted in the cochlea (± 6°; International Team for Ear Research, 1989, chapter 21; -15° to 20°; Ulfendahl et al., 1995). The differences in the observed motions are small for these small viewing angles, so that the numerical conditions for calculation of the 3D motion are poor. Mechanical instabilities in the preparation will compound the problem (see the Appendix).

To allow precise rotation of the object without losing the desired measurement spot, the ITER (1989, chapter 7) mounted a three-axial linear positioning system on a goniometer-system. The complete positioning system is too large and too heavy to integrate into a standard microscope. The need for a precision positioning and rotation system makes it difficult to adopt the measurement procedure de-

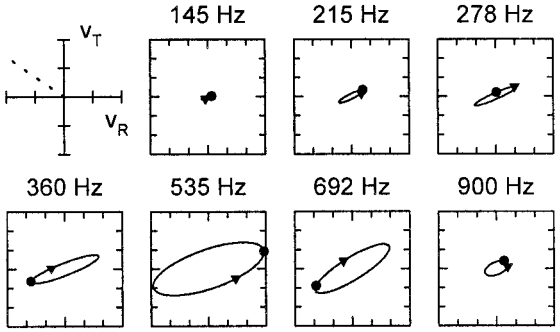

FIGURE 10 Velocity trajectories of a microsphere on the TM in the R–T-plane at different frequencies. Data are from Fig. 9. Inclination of the RL to the R-axis was 145° (*dotted line*). The scale bars extend to ±0.6 μm/s.

scribed by Decraemer et al. (1994) for a wider application range. To resolve these problems, a laser system, sensitive enough for recordings in the cochlea, which also detects motion in the plane orthogonal to the transverse direction, would be of great interest.

Accuracy and reliability of the recordings

The accuracy of the vibrations recorded with the LDV is only limited by the signal to noise ratio (SNR) of the measurement. In the temporal-bone preparation, the SNR in the middle frequency region (100–1000 Hz) is much greater than 20 dB, so that the amplitude and phase errors were less than 1 dB and 6°, respectively (Appendix). At lower and higher frequencies however, the SNR decreases, limiting the measurement range.

If it were possible to rotate the object through large angles, ideally 90°, then clearly the superior precision and sensitivity of the LDV compared with a photodiode would make it the measurement technique of choice. However, when the recording angle is limited, the calculation of the vibration direction is numerically ill-conditioned. If the rotation is 15°, minor inaccuracies in the amplitudes (±0.2 dB) or phases (±1.5°) give rise to an error in the calculated vibration angle of ±5°, or an ellipsoid that is 10% opened, respectively (Appendix). Thus, the strong dependence of the calculated vibration pattern on measurement errors for limited viewing angles defeats the purpose of using a high precision laser vibrometer. This problem becomes eminent when the object is not sufficiently stable, small disturbances during measurement of the vibration responses at different angles giving rise to relatively large errors.

With the aid of a differential photodiode mounted in the focal plane of the microscope, it was possible to overcome the problem of limited recording angle. Because the orthogonal components of the motion are then recorded, reconstruction of the vibration direction is numerically well-conditioned. An estimation of error is possible by assuming linear motion of the object in the R–T plane with an angle of 45°. An amplitude inaccuracy of ±1 dB causes an error in the calculated angle of only ±3°. Phase errors cause a deviation from rectilinear motion, the trajectory becoming elliptical. For a phase inaccuracy of ±6°, the ellipse opens to 10%; for a ±45° phase error the trajectory becomes a circle.

The accuracy of the vibration measurements presented in the present study was primarily limited by a slow drift of the measurement object (<30 μm/h), potentially causing a change of the photodiode sensitivity during the recordings. This deviation was assessed by measuring the photodiode sensitivity before and after recording of the frequency response. The number of frequency-response averages was limited to 20 as a compromise between stability and SNR.

Another potential source of error was possible changes in the condition of the temporal-bone preparation. The vibration response in the transverse direction was therefore measured before and after recordings with the photodiode. In most preparations, the amplitude of the responses decreased with time (<18 dB/h), probably due to a frequency-independent (below 1 kHz) stiffening of the middle ear (Hemmert et al., 2000). There was usually little change in the phase response (<5°). Preparations in which the shapes—not only the amplitudes—of the response functions changed with time were discarded.

Frequency response measurements

Biological systems often have a limited dynamic range and show pronounced nonlinearities. For frequency-response measurements it is important not to exceed the linear range of the system. Therefore, frequency response functions of the hearing organ are commonly determined with sinusoidal stimuli. However, using sinusoids with a sufficiently high resolution requires long recording times (ITER, 1989; chapter 9: 50 Hz–2 kHz in 25-Hz steps: 3½ min.). Therefore, broad-band signals, such as clicks (Robles et al., 1976), white noise (Hemmert et al., 2000; Preyer et al., 1994, 1996; Recio et al., 1997) or ternary white noise (Dallos and Santos-Sacchi, 1983; Dallos and Evans, 1995) are often used, which allow the determination of the complete frequency response within one measurement.

In systems that are essentially linear, as, for example, the middle ear (distortion ≪ 1% for levels < 80 dB SPL; Decraemer et al., 1994) and the temporal-bone preparation (distortion ≪ 1% for levels < 80 dB SPL, ITER, 1989), broad-band signals may be applied without causing significant distortion. The high linearity of the LDV allows the use of band-limited white noise. For the photodiode recordings, with its limited dynamic range, a multitone signal with 9.1 spectral lines per octave was developed. The advantage of this signal is its greatly reduced amplitude (⅓) and energy (1/12) compared with band-limited white noise. Distortion products fall between the logarithmically spaced

frequencies of the stimulus and, thus, compromise the measured response function less, compared with white noise. A complete frequency response function can be measured within a few seconds (20 averages: 4 s) using these broadband stimuli.

3D vibration of the cochlear partition

Responses measured in the transverse direction on a radial section of the organ of Corti demonstrated similar tuning characteristics for the Hensen cells, the three rows of outer hair cells, the inner hair cells (ITER, 1989), and the BM (Cooper and Rhode, 1995; 1996; Gummer et al., 1993; Hemmert et al., 2000). From the relative amplitudes and the small phase differences, it was concluded that the organ of Corti vibrates as a rigid body for frequencies below CF and that its motion is driven by the BM (von Békésy, 1960; Hemmert et al., 2000). The frequency-response curves compared well with those of in-vivo AC receptor-potential measurements from inner hair cells (Dallos, 1986) and recordings from nerve fibres (Evans, 1972; Rose et al., 1971) at low and medium sound levels. The refined measurement technique used in this study allowed, for the first time, a detailed study of the 3D motion of the cochlear partition. The results indicate that the motion of both BM and reticular lamina is predominantly orthogonal to their surfaces. Together with the small phase deviation between the vibration components, one can conclude that the organ of Corti, bounded by the reticular lamina and BM, rotates about a point near the edge of the inner limbus (Fig. 11).

Our results contradict findings by Ulfendahl et al. (1995), who reported relatively large phase differences between the transverse and radial vibration components of the RL but almost no difference for the TM. Therefore, in contrast to the almost rectilinear motion reported here for the BM and the RL, the trajectories reported by them were elliptical. This indicates the presence of a second mode of vibration of the RL in their experiments. The fact that the motion of the TM did not follow the motion of the RL at very low frequencies in their study may indicate that the TM was mechanically detached or altered by the perilymph, which flushed scala media when Reissner's membrane was opened. The results of the present study, using artificial endolymph as the bathing medium, indicate that the motion of the reticular and BMs was unimodal, at least up to CF. Our finding is in harmony with theoretic considerations: at least for frequencies well below CF, where presumably the motion of the cochlear partition is governed solely by its stiffness, only one vibration mode is expected.

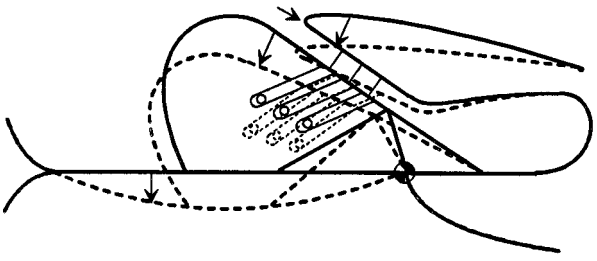

FIGURE 11 Vibration of the cochlear partition. The 3D vibration measurements (*arrows*, directions from Fig. 4 to Fig. 10) revealed that the organ of Corti bounded by the RL and BM rotates as a rigid body about a point near the inner limbus (rotation axes: ◒) for frequencies below CF. However, a second mode became evident in the vibration of the tectorial membrane for frequencies above ~0.5 oct below CF. This mode is parallel to the RL and presumably controls the deflection of the bundles of the outer hair cells.

In contrast to the situation for the BM and RL, recordings on the TM showed significant phase differences between the radial and the transverse components in the frequency range beginning ~0.5 oct below CF (Fig. 9; also Gummer et al., 1996). The vibration trajectories were near circular between this 0.5-oct frequency and CF (Fig. 10). This was not caused by a time-dependent change in the tuning properties of the cochlear partition, because there was no significant phase change in the transverse component during the recordings. Ulfendahl et al. (1995) reported almost rectilinear trajectories for the vibration of the TM. Apart from the problems associated with measurements along nonorthogonal axes, there might be an important physiologic reason for Ulfendahl's finding of rectilinear motion. Namely, if the second vibration mode is caused by a parallel resonance of the inertia of the TM with the bending stiffness of the hair bundle of outer hair cells, as suggested by Zwislocki and Kletzky (1979), then detachment of the TM from the hair bundle might be expected to not only destroy the resonant condition, but also cause the radial component to be reduced relative to the transverse component, so that the motion degenerates from elliptical to rectilinear. In contrast, if the physical coupling of the TM to the stiffness-dominated hair bundles of the outer hair cells were intact, the motion of the TM would be expected to follow the motion of the RL only at frequencies well below CF. This is definitively not the case in the report of Ulfendahl et al. (1995). Control experiments in an in-vivo preparation will be required to resolve this point. In the report by Gummer et al. (1996), the direction of the vibration trajectories changed dramatically: they appeared to rotate by more than 270° in a frequency range from 300 to 1000 Hz. This is because those recordings were not corrected for the open cochlea condition, known to produce a so-called fast component (Cooper and Rhode, 1996). The uncorrected frequency responses suggested a complicated 3D vibration pattern in which the relative motion between RL and TM appeared much more pronounced than for the slow component alone (Gummer et al., 1996). Moreover, model calculations by de Boer (1990) predicted that the open cochlea condition will emphasize vibration modes within the organ of Corti. When the response of the TM is corrected for the open cochlea condition, the phase difference between the

radial and transverse component does not exceed 90° and the vibration pattern is similar to the data published in Figs. 9 and 10. Nevertheless, the existence of a second degree of freedom in the motion of the TM parallel to the RL, the essence of the paper by Gummer et al. (1996), remains unchanged.

APPENDIX: ACCURACY OF 3D VIBRATION MEASUREMENTS

Alterations in the vibration trajectories resulting from measurement errors are estimated in this section. The errors produced by our measurement technique are compared with those produced by other techniques used in auditory physiology (Decraemer et al., 1994). In those techniques, vibration measurements are made in different but nonorthogonal directions. For simplicity, we will only examine the two-dimensional case, although the analysis is readily extended to three dimensions.

Assume harmonic oscillation:

$$\vec{\underline{v}}(t) = \vec{\underline{H}}e^{j\omega t} + \vec{\underline{T}}e^{j\omega t}, \tag{A1}$$

$\vec{\underline{H}}$ = complex amplitude of the horizontal vibration vector
$\vec{\underline{T}}$ = complex amplitude of the transversal vibration vector
j = $\sqrt{-1}$ imaginary number
ω = angular frequency
$e^{j\omega t}$ = $\cos(\omega t) + j\sin(\omega t)$ complex exponential function.

Without loss of generality, let the first measurement, $\underline{v}_1(t)$, be only of the transverse component, $\underline{T}$. That is, let

$$\underline{v}_1(t) = \underline{T}e^{j\omega t}. \tag{A2}$$

For the second measurement, $\underline{v}_2$ (t), the object is rotated by an angle of γ, so that

$$\underline{v}_2(t) = \underline{H}\sin(\gamma)e^{j\omega t} + \underline{T}\cos(\gamma)e^{j\omega t}. \tag{A3}$$

Eqs. A2 and A3 are readily solved to give the horizontal component,

$$\underline{H} = \frac{\underline{v}_2 - \underline{v}_1\cos(\gamma)}{\sin(\gamma)e^{j\omega t}}. \tag{A4}$$

For simplicity, we consider only the case where $\underline{H} = 0$ (rectilinear motion in the T-direction) and treat the cases of amplitude and phase errors in succession.

Assume a relative error, ε, in the amplitude of the second measurement:

$$\underline{v}_1(t) = \underline{T}e^{j\omega t}, \tag{A5}$$

$$\underline{v}_2(t) = (1+\varepsilon)\underline{T}\cos(\gamma)e^{j\omega t}. \tag{A6}$$

Then, the apparent horizontal component $\underline{H}'$ is

$$\underline{H}' = \frac{(1+\varepsilon)\underline{T}\cos(\gamma)e^{j\omega t} - \underline{T}\cos(\gamma)e^{j\omega t}}{\sin(\gamma)e^{j\omega t}} = \frac{\varepsilon}{\tan(\gamma)}\underline{T}. \tag{A7}$$

This error is critical if the object is accessible only from a limited angle γ, because the error is increased by a factor of $1/\tan(\gamma)$, which becomes large for small angles γ (e.g., the factor is 3.7 for $\gamma = 15°$). This error is equivalent to cross-talk between the transverse and horizontal components. For a measurement error or an instability of the preparation of only 1 dB ($\epsilon = 0.12$) and a rotation of the object of $\gamma = 15°$, the apparent horizontal component $\underline{H}'$ lies only 6.8 dB below the transverse component (see also Table A1). This causes a deviation of the reconstructed direction of the major axis of the trajectory of 24.5°.

TABLE A1 Cross-talk between the transverse and the horizontal components and corresponding deviation of the reconstructed vibration direction for a relative error ε in the amplitude measurement of an object in rectilinear motion ($\underline{H} = 0$), where the difference between the measurement directions is $\gamma = 15°$.

Relative Amplitude Error ε (dB)	Cross-talk (dB)	Deviation of Vibration Trajectory (degrees)
0.2	−21.2	5.0
0.3	−17.6	7.5
0.5	−13.1	12.5
1.0	−6.8	24.5
2.0	−0.3	44.0
3.0	+3.7	57.0

Consider next the effect of an absolute phase error, δ, in the measurement of $\underline{v}_2$. Again for rectilinear motion ($H = 0$), the apparent value of the horizontal component is

$$\underline{H}' = \frac{\underline{T}\cos(\gamma)e^{j(\omega t+\delta)} - \underline{T}\cos(\gamma)e^{j\omega t}}{\sin(\gamma)e^{j\omega t}} = \frac{e^{j\delta}-1}{\tan(\gamma)}\underline{T}. \tag{A8}$$

For an absolute phase error $\delta = 5°$ (and $\gamma = 15°$), the apparent amplitude of the imaginary part of $\underline{H}'$ is only 9.7 dB below the transverse component $\underline{T}$. Moreover, this means that the apparent component $\underline{H}'$ is almost 90° (87.5°) phase-shifted relative to the $\underline{T}$-component, causing an apparent elliptical trajectory. The apparent opening of the elliptical trajectory,

$$\left(\frac{\sin(\delta)}{\tan(\gamma)}\middle/1 + \frac{|\cos(\delta)-1|}{\tan(\gamma)}\right)\cdot 100\%$$

(defined as the ratio of the length of the minor axis to the length of the major axes), is 32% (see also Table A2).

Therefore, to achieve reliable two- or three-dimensional vibration data when the observation angle of a measurement object is restricted, high demands on the measurement precision must be made. If cross-talk of less than 10% is required, phase errors must be $\delta < 1.5°$ and the precision of the amplitude must be better than 0.2 dB. In this respect, it is also necessary that the measurement object be extremely stable.

TABLE A2 Cross-talk between the transverse and horizontal components, deviation of the reconstructed vibration direction and apparent opening of the elliptical trajectory of the vibration for an absolute error δ in the phase measurement of an object in rectilinear motion ($\underline{H} = 0$), where the difference between the measurement directions is $\gamma = 15°$.

Absolute Phase Error δ (degrees)	Cross-talk (dB)	Deviation of Vibration Trajectory (degrees)	Opening of Ellipse (%)
1	−23.7	0.03	6.5
1.5	−20.2	0.07	10
3	−14.2	0.29	19
5	−9.7	0.81	32
10	−3.7	3.2	61

For the case where the orthogonal vibration components are directly measured, the calculation of the alterations of the trajectories can be straightforward. We will consider two cases:

Case 1: $\underline{H} = 0$, rectilinear motion in the T-direction (90°). A relative error ϵ in the measurement of the amplitude of the transverse component will remain as an error ϵ in the apparent value of the component, whereas an absolute phase error δ of 10° will cause an elliptical trajectory with an opening of 18%. The direction of the trajectory will be altered for cross-talk between the transverse and horizontal components. Cross-talk of 10% will cause a deviation of the vibration direction of 5.7°.

Case 2: $\underline{H} = \underline{T}$ rectilinear motion at an angle of 45° to the coordinate axes. An amplitude error of 3 dB in the measurement of one component leads to a deviation of the vibration direction of 9.7°; a phase error of 10° in the measurement of one component will cause an elliptical trajectory with an artificial opening of 17%.

These comparisons show that the direct measurement of the orthogonal vibration components is much less sensitive to measurement errors. In contrast, when the measurement object is accessible only from a limited angle, as it is in the case for middle-ear measurements or for recordings in the cochlea, small measurement errors cause relatively large deviations in the apparent vibration direction and in the form of the trajectories.

We are grateful for the technical assistance of Bernd Maier and Annegret Seeger. We also acknowledge the contributions made by the reviewers.

This work was supported by the Deutsche Forschungsgemeinschaft, Sonderforschungsbereich 307, Teilprojekt C10. We thank also the Helmholtzstiftung and the Humboldt Foundation for their additional support provided to W.H.

REFERENCES

Allen, J. B. 1980. Cochlear micromechanics—a physical model of transduction. *J. Acoust. Soc. Am.* 68:1660–1670.

Bosher, S. K. 1979. The nature of the negative endocochlear potentials produced by anoxia and ethacrynic acid in the rat and guinea pig. *J. Physiol.* 293:329–345.

Brownell, W. E., C. R. Bader, D. Bertrand, and Y. de Ribaupierre. 1985. Evoked mechanical responses of isolated cochlear outer hair cells. *Science.* 227:194–196.

Cooper, N. P., and W. S. Rhode. 1993. Nonlinear mechanics at the base and apex of the mammalian cochlea: in-vivo observations using a displacement-sensitive laser interferometer. *In* Biophysics of Hair Cell Sensory Systems. H. Duifhuis, J. W. Horst, P. van Dijk, and S. M. van Netten, editors. World Scientific, Singapore, New Jersey, London, Hong Kong. 229–236.

Cooper, N. P., and W. S. Rhode. 1995. Nonlinear mechanics at the apex of the guinea-pig cochlea. *Hear. Res.* 82:225–243.

Cooper, N. P., and W. S. Rhode. 1996. Fast travelling waves, slow travelling waves and their interactions in experimental studies of apical cochlear mechanics. *Aud. Neurosci.* 2:289–299.

Dallos, P. 1986. Neurobiology of cochlear inner and outer hair cells: intracellular recordings. *Hear. Res.* 22:185–198.

Dallos, P., and B. N. Evans. 1995. High-frequency motility of outer hair cells and the cochlear amplifier. *Science.* 267:2006–2009.

Dallos, P., and J. Santos-Sacchi. 1983. AC receptor potentials from hair cells in the low-frequency region of the guinea pig cochlea. *In* Mechanisms of Hearing. W. R. Webster and L. M. Aitkin, editors. Monash University Press, Clayton, Victoria, Australia. 11–16.

de Boer, E. 1990. Wave-propagation modes and boundary conditions for the Ulfendahl–Flock–Khanna preparation. *In* The Mechanics and Biophysics of Hearing. P. Dallos, C. P. Geisler, J. W. Matthews, M. A. Ruggero, and C. R. Steele, editors. Springer-Verlag, Berlin, Heidelberg. 333–339.

Decraemer, W. F., S. M. Khanna, and W. R. J. Funnell. 1994. A method for determining three-dimensional vibration in the ear. *Hear. Res.* 77: 19–37.

Evans, E. F. 1972. The frequency response and other properties of single fibres in the guinea-pig cochlear nerve. *J. Physiol. (Lond.).* 226: 263–287.

Frank, G., W. Hemmert, and H.-P. Zenner. 1999. Limiting dynamics of high-frequency electromechanical transduction of outer hair cells. *Proc. Natl. Acad. Sci. USA.* 96:4420–4425.

Gitter, A. H., and H. P. Zenner. 1995. Electromotile responses and frequency tuning of isolated outer hair cells of the guinea pig cochlea. *Eur. Arch. Otorhinolaryngol.* 252:15–19.

Gummer, A. W., W. Hemmert, I. Morioka, P. Reis, G. Reuter, and H. P. Zenner. 1993. Cellular motility measured in the guinea-pig cochlea. *In* Biophysics of Hair Cell Sensory Systems. H. Duifhuis, J. W. Horst, P. van Dijk, and S. M. van Netten, editors. World Scientific, Singapore, New Jersey, London, Hong Kong. 229–236.

Gummer, A. W., W. Hemmert, and H.-P. Zenner. 1996. Resonant tectorial-membrane motion in the inner ear: its crucial role in frequency tuning. *Proc. Natl. Acad. Sci. USA.* 93:8727–8732.

Gummer, A. W., J. W. T. Smolders, and R. Klinke. 1987. Basilar membrane motion in the pigeon measured with the Mössbauer technique. *Hear. Res.* 29:63–92.

Hao, L. F., and S. M. Khanna. 1996. Reissner's membrane vibrations in the apical turn of a living guinea pig cochlea. *Hear. Res.* 99:176–189.

Hemmert, W., H.-P. Zenner, and A. W. Gummer. 1995. Three-dimensional vibration measurements on different locations of the cochlear partition. *Proc. 18th ARO Midwinter Meeting*, 5–9 February 1995, St. Petersburg Beach, Fla. Association for Research in Otolaryngology, 448. (Abstr.).

Hemmert, W., H.-P. Zenner, and A. W. Gummer. 1997. Three-dimensional vibration of the cochlear partition: correction for the open cochlea condition. *Proc. 20th ARO Midwinter Meeting*, 2–6 February 1997, St. Petersburg Beach, Fla. Association for Research in Otolaryngology, 40. (Abstr.).

Hemmert, W., H.-P. Zenner, and A. W. Gummer. 2000. Characteristics of the travelling wave in the low-frequency region of a temporal-bone preparation of the guinea-pig cochlea. *Hear. Res.* 142:184–202.

International Team for Ear Research. 1989. Cellular vibration and motility in the organ of Corti. *Acta Oto-Laryngol. Suppl.* 467:5–279.

Kolston, P. J., and J. F. Ashmore. 1996. Finite element micromechanical modeling of the cochlea in three dimensions. *J. Acoust. Soc. Am.* 99: 455–467.

Kronester-Frei, A. 1979. The effect of changes in endolymphatic ion concentrations on the tectorial membrane. *Hear. Res.* 1:81–94.

Kros. C. J., A. Rüsch, and G. P. Richardson. 1992. Mechano-electrical transducer currents in hair cells of the cultured neonatal mouse. *Proc. R. Soc. Lond. B.* 249:185–193.

Lim, D. J. 1980. Cochlear anatomy related to cochlear micromechanics: a review. *J. Acoust. Soc. Am.* 67:1686–1695.

Maier, H., C. Zinn, A. Rothe, H. Tiziani, and A. W. Gummer. 1997. Development of a narrow water-immersion objective for laserinterferometric and electrophysiological applications in cell biology. *J. Neurosci. Meth.* 77:31–41.

Neely, S. T., and L. J. Stover. 1993. Otoacoustic emissions from a nonlinear, active model of cochlear mechanics. *In* Biophysics of Hair Cell Sensory Systems. H. Duifhuis, J. W. Horst, P. van Dijk, S. M. van Netten, editors. World Scientific, Singapore, New Jersey, London, Hong Kong. 229–236.

Nobili, R., and F. Mammano. 1996. Biophysics of the cochlea. II. Stationary nonlinear phenomenology. *J. Acoust. Soc. Am.* 99:2244–2255.

Preyer, S., W. Hemmert, M. Pfister, H.-P. Zenner, and A. W. Gummer. 1994. Frequency response of mature guinea-pig outer hair cells to stereociliary displacement. *Hear. Res.* 77:116–124.

Preyer, S., S. Renz, W. Hemmert, H.-P. Zenner, and A. W. Gummer. 1996. Receptor potential of outer hair cells isolated from base to apex of the adult guinea-pig cochlea: implications for cochlear tuning mechanisms. *Aud. Neurosci.* 2:145–157.

Recio, A., S. S. Narayan, and M. A. Ruggero. 1997. Wiener–Kernel analysis of basilar-membrane responses to white noise. *In* Diversity in Auditory Mechanics. E. R. Lewis, G. R. Long, R. F. Lyon, P. M. Narins, C. R. Steele, and E. Hecht-Poinar, editors. World Scientific, Singapore, New Jersey, London, Hong Kong. 325–331.

Rhode, W. S., and N. P. Cooper. 1996. Nonlinear mechanics in the apical turn of the chinchilla cochlea in vivo. *Aud. Neurosci.* 3:101–121.

Rhode, W. S., and C. D. Geisler. 1967. Model of the displacement between opposing points on the tectorial membrane and reticular lamina. *J. Acoust. Soc. Am.* 42:185–190.

Robles, L., W. S. Rhode, and C. D. Geisler. 1976. Transient response of the basilar membrane measured in squirrel monkeys using the Mössbauer effect. *J. Acoust. Soc. Am.* 59:926–939.

Rose, J. E., J. E. Hind, D. J. Anderson, and J. F. Brugge. 1971. Some effects of stimulus intensity on response of auditory nerve fibers in the squirrel monkey. *J. Neurophysiol.* 34:685–699.

ter Kuile, E. 1900. Die Übertragung der Energie von der Grundmembran auf die Haarzelle. *Arch. ges. Physiol.* 79:146–156.

Ulfendahl, M., S. M. Khanna, A. Fridberger, Å. Flock, B. Flock, and W. Jäger. 1996. Mechanical response characteristics of the hearing organ in the low-frequency regions of the cochlea. *J. Neurophysiol.* 76: 3850–3862.

Ulfendahl, M., S. M. Khanna, and C. Heneghan. 1995. Shearing motion in the hearing organ measured by confocal laser heterodyne interferometry. *Neuroreport.* 6:1157–1160.

Voldřich, L. 1983. Experimental, and topographic morphology in cochlear mechanics. *In* Mechanics of Hearing. E. de Boer, and M. A. Viergever, editors. Martinus Nijhoff Publishers and Delft University Press, Delft, The Netherlands. 163–167.

von Békésy, G. 1960. Experiments in Hearing. McGraw-Hill, New York.

Wilson, J. P., and J. R. Johnstone. 1975. Basilar membrane and middle-ear vibration in guinea pig measured by capacitive probe. *J. Acoust. Soc. Am.* 57:705–723.

Zenner, H. P., U. Zimmermann, and U. Schmitt. 1985. Reversible contraction of isolated mammalian cochlear hair cells. *Hear. Res.* 18:127–133.

Zinn, C., H. Maier, H.-P. Zenner, and A. W. Gummer. 2000. Evidence for active, nonlinear, negative feedback in the vibration response of the apical region of the in-vivo guinea-pig cochlea. *Hear. Res.* 142: 159–183.

Zwislocki, J. J. 1980. Five decades of research on cochlear mechanics. *J. Acoust. Soc. Am.* 67:1679–1685.

Zwislocki, J. J., and E. J. Kletsky. 1979. Tectorial membrane: a possible effect on frequency analysis in the cochlea. *Science.* 204:639–641.